Electronic structure of vacancy defects in MgO crystals

Q. S. Wang* and N. A. W. Holzwarth
Department of Physics, Wake Forest University, P.O. Box 7507, Reynolda Station, Winston-Salem, North Carolina 27109
(Received 14 August 1989)

The electronic structure of oxygen-vacancy defects (F, F^+ and F^{2+} centers) in MgO crystals has been studied within local-density theory, using the self-consistent mixed-basis pseudopotential techniques. The defects were modeled within a supercell having a volume 8 times that of the perfect MgO crystal. The band structure, density of states, charge-density contours, and total energy were calculated as a function of lattice relaxation. The partial density of states shows that each of the F-type centers introduces impurity states into the band gap as well as near the conduction-band edge of MgO. The total energy was calculated as a function of relaxation of the nearest-neighbor shell of Mg^{2+} ions. For F centers, the lowest-energy configuration was found to be a small inward relaxation of the nearest Mg^{2+} ions toward the vacancy site. For F^+ and F^{2+} centers, the lowest total energies correspond to a small outward relaxation of the Mg^{2+} ions away from the vacancy site. The electronic structure of hydrogen impurities (H^- and H^{2-} substitutional defects) in MgO was also investigated using the same approach. These impurities contribute defect states within and below the oxygen p bands as well as near the conduction-band edge of MgO. The lowest-total-energy configurations of both H^- and H^{2-} substitutional defects correspond to a slight outward relaxation of the nearest Mg^{2+}-ion shell.

I. INTRODUCTION

Point defects occur naturally and by design in insulating and semiconducting crystals, producing interesting optical and electrical properties. Several types of defect structures have been identified and studied in the alkaline-earth oxide material MgO.[1,2] Although this material has been studied for more than 20 years, some fundamental questions still remain. In particular, Chen and Summers at Oak Ridge National Laboratories and their collaborators[3–9] have carried out a series of experimental studies of luminescence from states associated with the oxygen vacancy in MgO. Earlier work, together with recent time-resolved measurements of this luminescence by Rosenblatt, Rowe, Williams, Williams, and Chen,[9] has helped develop a simple model for this system. In the present paper we examine the various ingredients of this model from the framework of density-functional theory using mixed-basis pseudopotential techniques.

According to the model, the experimental situation is explained as follows and illustrated schematically in Fig. 1. An oxygen vacancy forms a bound state in the band gap of MgO, which, in the ground state, contains two electrons. This neutral defect is known as an F center. The F center can absorb a broad band of radiation with peak absorption at 5 eV forming various excited bound states F^*.[5] Aside from nonradiative-decay processes, the F^* defect can do either of two things—luminesce or ionize. In the former case because of lattice relaxation, the luminescent radiation is 2 eV. In the latter case the excited electron enters the conduction band of MgO, leaving the defect with a single bound electron, denoted an F^+ center. The F^+ center can now absorb a broad band of radiation with peak absorption at 5 eV forming various excited bound states F^{+*}. Aside from nonradiative-decay processes, the F^{+*} defect can do either of two things—luminesce or ionize. In the former case, because of lattice relaxation, the luminescent radiation is 3 eV. In the latter case the excited electron enters the conduction band of MgO, leaving the defect with no bound electrons, denoted an F^{2+} center. The electrons released to the conduction band from the ionization processes $F^* \rightarrow F^+$ and $F^{+*} \rightarrow F^{2+}$ can be trapped at defect states near the conduction-band edge. One such trapping site has been shown to be a H^- substitutional defect, formed when a hydrogen atom, occupying an F^+-center site, is perturbed by a nearby impurity or vacancy. (Other hydrogen-containing defects can also exist.[8]) When the H^- substitutional defect (or a perturbed H^- substitutional defect) captures an electron, it becomes an overall neutral H^{2-} substitutional defect. Since the binding energy of the trap sites is comparable to thermal energies, the

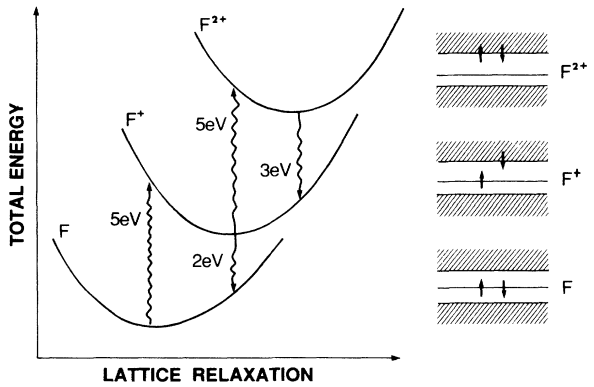

FIG. 1. Schematic configuration-coordinate diagrams for the F, F^+, (F^*), and F^{2+} (F^{+*}) centers in MgO, following the model discussed in Ref. 9. Franck-Condon photon processes are represented with wavy arrows. The corresponding one-electron diagrams are shown schematically on the right with occupancies indicated with small arrows representing electron-spin states. Band states are indicated in hatched regions, the lower (valence) band being filled in all three cases.

trap sites act as electron reservoirs for the F-like luminescent centers. Electrons released from the H^{2-} electron-trap sites to the conduction band can recombine with an F^{2+} center via $F^{2+}+e^{-}\rightarrow F^{+*}$, or can recombine with an F^{+} center via $F^{+}+e^{-}\rightarrow F^{*}$. In the former case, F^{+} luminescence at 3 eV is produced; in the latter case, F luminescence at 2 eV is produced. This model thus provides a mechanism for the very-long-lived luminescence observed[8,9] in these systems. Since the mechanism is highly sensitive to the number of trap sites available (the hydrogen concentration), to the rate at which electrons in the excited F^{*} and F^{+*} states are released to the conduction band (the temperature), and to the number of 5-eV photons available (incident light intensity), the model can be thoroughly tested. The measurements of Rosenblatt and co-workers[9] are in qualitative support of the model.

The main features of the model are illustrated in Fig. 1 both from the viewpoint of the total energy of the system as a function of lattice relaxation (configuration-coordinate diagram[1]) shown on the left panel and from the viewpoint of the corresponding one-electron states indicated in the right panel. In this diagram we have neglected the intermediate ionization steps $F^{*}\leftrightarrow F^{+}$ and $F^{+*}\leftrightarrow F^{2+}$. We also have neglected these steps in our calculations since, to a good approximation, the screening properties of the excited and ionized impurities, and hence the configuration-coordinate diagrams, are very similar. Had the bound F^{*} and F^{+*} states been included in the configuration-coordinate diagrams, they would appear as a series of closely spaced curves under the F^{+} and F^{2+} curves, respectively, similar to the configuration-coordinate diagrams given by Wilson and Wood[10] and by Summers, Wilson, Jeffries, Tohver, Chen, and Abraham.[5] Also omitted from the configuration-coordinate diagram of Fig. 1 is the representation of the ionization continua which would appear as a continuum of curves above the F^{+} curve and a continuum of curves above the F^{2+} curve, representing the total energies corresponding to possible occupancies of the one-electron states in the conduction bands. The F and F^{+} portions of the model have been well described in the literature.[5] However, the F^{2+} states seems to be less well accepted.[2,9,11,12]

There have been a number of theoretical studies of some of the oxygen vacancies and hydrogenated oxygen vacancies in MgO crystals. This work has focused *either* on the one-electron energy spectrum *or* on the configuration-coordinate diagram determined from the total energy of the defect system as a function of the static nuclear positions. From the one-electron viewpoint, Klein, Pickett, Boyer, and Zeller[13] have carried out a muffin-tin Green's-function calculation of F and F^{+} sites in MgO crystals. They were able to locate the defect states with respect to the band edges of MgO within the local-density approximation in the perfect-crystal geometry. Their results were consistent with the experimental evidence that the excited states of F and F^{+} are close to the conduction-band edge of MgO. From the total-energy viewpoint, Pandey and Vail[14,15] have carried out embedded-cluster calculations of F, F^{+}, H^{-}, and H^{2-} defects, treating the cluster within the unrestricted Hartree-Fock approximation. The cluster was coupled to the rest of the lattice in terms of a self-consistent classical shell model. These authors determined the equilibrium geometry of the defects and their relaxation energies. In particular, they found that the nearest-neighbor Mg^{2+} ions relax by moving towards the F center and away from the F^{+}, H^{-}, and H^{2-} defects. The results of Pandey and Vail for the ground-state geometry of F is in contradiction to earler work by Summers, Wilson, Jeffries, Tohver, Chen, and Abraham[5] and of Wilson and Wood,[10,16] who calculated the configuration-coordinate diagram for F in its ground and excited states, finding the ground-state equilibrium geometry to correspond to an expansion of the nearest-neighbor Mg^{2+} positions away from the F center. This earlier work also made a detailed study of the configuration-coordinate diagrams of several bound excited states of the F center, using methods successfully developed for the study of F centers in alkali halide crystals.[17–19] It was based on a Hartree-Fock calculation for the defect-centered inner region and an effective-mass-approximation technique for the outer region of the crystals.

It is apparent that there is a need to develop a model which determines *both* the one-electron energies as well as the total energy of the system as a function of defect geometry, in order to make a detailed comparison with experiment. Density-functional theory[20] can do just that. The one-electron energies determined from density-functional theory provide a semiquantitative picture of the states of the system corresponding to the right panel of Fig. 1. By assigning occupancies for these states, the total energy of the system can be determined as a function of lattice geometry, and configuration-coordinate diagrams as shown in the left panel can be constructed.

In the present work,[21] we have carried out a systematic study of the ground state of the electronic structure and total energy of MgO and its F, F^{+}, F^{2+}, H^{-}, and H^{2-} defects. This study has been carried out using self-consistent mixed-basis pseudopotential techniques,[22] representing the defect in a supercell geometry. For each type of impurity, the electronic band structure, the corresponding density of one-electron states, charge-density contours, and configuration-coordinate diagrams were calculated.

The outline of the remaining portion of this paper is as follows. In Sec. II the calculational method is briefly presented. In Sec. III the results for the F, F^{+}, and F^{2+} defects are reported. The electronic structure of hydrogen impurities are presented in Sec. IV. The discussion and conclusions are given in Sec. V.

II. METHODS

A. Supercell geometry

MgO crystals have the NaCl structure with a face-centered-cubic (fcc) Bravais lattice. The cubic lattice constant is 4.21 Å.[23] In our defect studies, we have constructed a super unit cell by doubling the linear dimensions of the original unit cell of MgO. This corresponds to a supercell volume 8 times that of MgO and to a

stoichiometry of Mg_8O_7d. Taking the defect (oxygen vacancy or substitutional hydrogen) site d to be located at the origin, the unit cell contains six nearest-neighbor magnesium atoms plus two magnesium and seven oxygen atoms located on the boundaries of the supercell.

B. Band structure

It is well established that Hohenberg-Kohn-Sham density-functional theory,[20] in the Hedin-Lundqvist parametrization of the local-density approximation,[24] using mixed-basis pseudopotential techniques,[22,25–29] provides an accurate and efficient method for determining the ground-state electronic structure of complex systems. These techniques have been successfully used by several groups.

Operationally, the procedure consists of the following four steps. First, we find the norm-conserving ionic pseudopotentials,[26] using Kerker's functional form,[27] modified to include non-spin-orbit relativistic effects[28,29] and the exchange-correlation effects of the approximate core density.[25] In the present work, the pseudopotential radii were chosen to be 2.4 bohr for Mg (s and p orbitals), 1.0 bohr for O (s and p orbitals), and 1.1 bohr for H (s orbital only). Secondly, we form the ionic crystal potential and an approximate valence-electron density $\rho(\mathbf{r})$ and its corresponding Hartree $V_H(\mathbf{r})$ and exchange-correlation $V_{xc}(\rho(\mathbf{r}))$ potentials. In performing the band-structure calculation, it is generally convenient to take the zero of energy as the average value (or, equivalently, the $G=0$ term) of the sum of the ionic and Hartree potentials. Thirdly, the band-structure calculation is performed at representative values of wave vector $\mathbf{k}$ throughout the Brillouin zone using mixed-basis wave functions of the form

$$\Psi_n(\mathbf{k},\mathbf{r})=\sum_G \alpha_n^G(\mathbf{k})\exp[i(\mathbf{k}+\mathbf{G})\cdot\mathbf{r}]+\sum_\mu \beta_n^\mu(\mathbf{k})\Phi^\mu(\mathbf{k},\mathbf{r}) \ . \tag{1}$$

In this expansion, $\mathbf{G}$ denotes a reciprocal-lattice vector of the plane-wave function and $\Phi^\mu(\mathbf{k},\mathbf{r})$ denotes a linear combination of atomic orbitals (LCAO) function with μ representing site and orbital-type index. The coefficients $\alpha_n^G(\mathbf{k})$ of the plane-wave contributions and $\beta_n^\mu(\mathbf{k})$ of the LCAO contributions are determined by solving a generalized eigenvalue problem of the form

$$(H-\varepsilon_{n\mathbf{k}}S)\Lambda=0, \quad \Lambda=\begin{pmatrix}\alpha\\ \beta\end{pmatrix} \ . \tag{2}$$

Here, H and S are the Hamiltonian and overlap matrices, respectively, and $\varepsilon_{n\mathbf{k}}$ denotes the one-electron eigenvalues. We have found that it is generally most efficient to form the LCAO functions from the valence atomic pseudopotential wave functions. Then, the number of plane waves needed to accurately represent the wave function (1), in order to represent the shape changes in the atomic function which occur primarily in the valence region, can be kept to a manageable size. In the present study, LCAO functions were included in the basis set of O s-like, O p-like, and H s-like orbitals. The valence states of Mg and of the vacancy were adequately represented by the plane-wave basis functions. The reciprocal-lattice sums were calculated by including all reciprocal-lattice vectors such that $|\mathbf{G}|^2\le 121$ bohr^{-2}, corresponding to 22 659 vectors; the cutoff energies for the plane-wave basis functions were $|\mathbf{k}+\mathbf{G}|^2\le 8$ bohr^{-2} and, for representing the LCAO functions, $|\mathbf{k}+\mathbf{G}|^2\le 100$ bohr^{-2}, corresponding to approximately 400 and 17 000 vectors, respectively. These choices for cutoff energies were a compromise between ideal convergence and reasonable numbers of reciprocal-lattice vectors; they ensured the energy eigenvalues to be converged within 0.1 eV and the total energies to be converged within 0.5 eV. The fourth step is to form the charge density corresponding to the band-structure results:

$$\rho(\mathbf{r})=\sum_{n,\mathbf{k}} w_{n\mathbf{k}}|\Psi_n(\mathbf{k},\mathbf{r})|^2 \ . \tag{3}$$

Here $w_{n\mathbf{k}}$ represents the weight and occupancy factor for the nth band of wave vector $\mathbf{k}$. The $\mathbf{k}$ points used in the summation (3) were the same as those used to calculated the density of states as explained below. From this charge density, the new $\rho(\mathbf{r})$ is used to determine the new Hartree and exchange-correlation potentials, and steps 3 and 4 are iterated to self-consistency.

The self-consistent band-structure calculations required the most computer time for this study. In the final stages of this work, these calculations were performed on a Convex C120 computer, requiring approximately 1 day of computation to converge each lattice geometry. The majority of the project was carried out on a Prime 1451 computer and a Sun 3/50 work station with 4–8 times longer computation times.

Once the self-consistent electronic structure has been determined, the one-electron picture can be completed by determining the band structure along symmetry directions in the Brillouin zone and by determining the density of states.

C. Density of states

The density of states (DOS)

$$N(E)=\sum_n \int d^3k\ \delta(E-\varepsilon_{n\mathbf{k}}) \tag{4}$$

and the ith partial density of states (PDOS)

$$N^i(E)=\sum_n \int d^3k\ f_n^i(\mathbf{k})\delta(E-\varepsilon_{n\mathbf{k}}) \tag{5}$$

were calculated from the energy bands and their gradients, using the Gilat-Raubenheimer-Kam method.[30,31] The gradients of the energy bands were calculated[32] using the Hellmann-Feynman theorem.[33] We chose the $\mathbf{k}$-space sampling by dividing the reciprocal-lattice unit cell for the supercell into $3\times3\times3$ parallelepipeds. The sampling $\mathbf{k}$ points are taken at the midpoints of each of the parallelepipeds, which corresponds to six nonequivalent $\mathbf{k}$ points in the first Brillouin zone of the supercell. (The equivalent sampling of MgO divides the reciprocal-lattice unit cell into $6\times6\times6$ parallelepipeds corresponding to 28 nonequivalent $\mathbf{k}$ points.) The evaluation was performed at each of the sampling $\mathbf{k}$ points for all the energy bands. In the PDOS calculations, the weight factors of type i

were taken as the fraction of charge associated with each band n within spheres centered at the defect sites. In the present work the sphere radius was chosen to be 1.98 bohr (one-half the nearest-neighbor distance), corresponding to a fractional volume of 0.03 for calculating the PDOS for the defect sites. While this volume is too small to enclose all of the impurity charge, it provides a qualitative measure of the impurity contribution to the density of states.

D. Total energy

The total energy of the system was evaluated in momentum space according to the formalism developed by Ihm, Zunger, and Cohen.[34] The total energy per unit cell is given by

$$E_{\rm tot}=\sum_{n,\mathbf{k}} w_{n\mathbf{k}}\varepsilon_{n\mathbf{k}}-\tfrac{1}{2}\sum_{\mathbf{G}\,(\neq 0)} V_H(\mathbf{G})\rho(\mathbf{G}) + \sum_{G}[\varepsilon_{\rm xc}(\mathbf{G})-V_{\rm xc}(\mathbf{G})]\rho(\mathbf{G})+\alpha+\gamma\ . \quad (6)$$

Here, $\varepsilon_{\rm xc}(\rho)$ represents the total exchange-correlation energy functional, γ represents the Ewald energy[35] of the ion-ion interaction, and α represents a correction for the deviation of the pseudopotentials from point ions. The Ewald energy is calculated by screening the positive ion potentials with a uniform negative background charge. For a neutral system this uniform negative background charge is present as the $\mathbf{G}=0$ contribution of the electronic Coulomb term. For a charged system, additional terms must be added in order to avoid divergences as discussed briefly below. In order to study the effects of nuclear relaxation, the entire procedure can be repeated for a series of nuclear configurations, constructing a "configuration-coordinate" diagram. The nuclear geometry having the lowest energy corresponds to the ground state of the system.

E. Calculation for charged impurities

For the charged defect systems, F^+, F^{2+}, and H^-, special care is needed to avoid divergences in the total-energy calculations. Two different approaches were used to study these cases, which we refer to as the "ionized" treatment and the "excited" treatment.

In the "ionized" treatment we carry out the density-functional calculations for the system having a net positive charge ($+1|e|$/unit-cell for F^+, $+2|e|$/unit-cell for F^{2+}, and $+1|e|$/unit-cell for H^-). This procedure is well defined for the band-structure calculation since the net charge of the system only affects the $\mathbf{G}=0$ value of the Coulombic contribution to the potential, which we set equal to 0 by our choice of the zero of band energy. However, the total energy diverges because of the infinite Coulomb energy of a system with a periodic array of charge. The difficulty can be overcome by performing the total-energy calculation for an appropriate neutral system. We have done this by using an approach suggested by Bar-Yam[36,37] as follows. In calculating the total energy we include, in an approximate way, the energetic effects of the electrons removed in forming the ionic states of the defect, assuming that these electrons occupy the lowest-conduction-band states and that they have a uniform spatial distribution. The uniform distribution of compensating electronic charge ensures that the Coulomb contribution to the total energy will be finite and it slightly alters the exchange-correlation contribution. An additional contribution to the total energy is approximated by including the one-electron energy terms, in Eq. (6), for the electrons added to the lowest conduction bands. In a sense, the ionized impurity states can be considered as excited states of the Mg_8O_7d system. In our "ionized" treatment, the excited-state considerations do not affect the self-consistency loop, but only enter the calculation of the total energy. Thus, our "ionized" treatment approximates the calculation of the self-consistent ground-state density of the ionized system. To the extent that the energy corrections are insensitive to the nuclear coordinates, they provide a nearly constant (although not entirely rigorous) energy shift to the configuration-coordinate diagram for the charged impurity.

In the "excited" treatment we perform a *bona fide* ΔSCF calculation.[38] In the ΔSCF approach, both the ground and excited states of the system are calculated self-consistently within density-functional theory and the excitation energy is determined by subtracting the total energies of the two configurations. This ΔSCF scheme is physically appealing, although it is not rigorously consistent with density-functional theory, which is strictly a ground-state theory. For the F^+ center the one-electron occupancies are adjusted so that there is one electron in the impurity band and one electron distributed within the conduction band. For the F^{2+} center there are no electrons in the impurity band and two electrons are distributed in the conduction band. For the H^- defect the situation is more complicated as explained below. The self-consistent local-density calculations are performed as described in Sec. II B with these occupancy constraints. Since the systems are neutral, the total energies can be calculated exactly from Eq. (6). Physically, this treatment differs from the "ionized" treatment in that the excited electrons are allowed to respond and screen the ionized impurity. To the extent that these excited electrons are in highly extended states, these screening effects are expected to be small.

In both treatments the comparison of the configuration-coordinate diagrams for the defect in each of its charge states can be related to experiment. For each nuclear geometry, the total-energy difference between the "ionized" or "excited" configuration and ground-state configuration is expected to approximate the electronic excitation energy. According to the Franck-Condon approximation,[1] the most probable photon absorption and luminescence processes can be estimated as vertical transitions from minima in the resulting configuration-coordinate diagrams. From this viewpoint the experimental energies are derived from the total-electronic-energy calculations. The one-electron energies with their famous band-gap problem[43] are not directly compared with experiment. We expect this local-density, total-

energy treatment to approximate some of the features of a full many-body analysis.[43]

III. ELECTRONIC STRUCTURE OF *F* CENTERS IN MgO

The starting point of this study was a calculation of the electronic structure of defect-free MgO crystals. Figure 2 shows the energy bands and the corresponding density of states for MgO. The occupied states of this band structure are a narrow oxygen *s* band, whose minimum at the Γ point was taken as the zero of energy, and, at 12 eV higher energy, the wider oxygen *p* band. The Mg *s* states mainly contribute to the conduction band, having minimum energy at the Γ point. As expected for an insulating crystal, there is a well-defined band gap between the oxygen *p* band and the conduction band. These results can be compared with those of Chang and Cohen[39] and with the experimental results they referenced.[40,41] Chang and Cohen focused on examining the structural and electronic properties of the high-pressure behavior of MgO. Their computational method differed from ours only in that they used a plane-wave basis, while we used a mixed LCAO and plane-wave basis. The comparison of the band characteristics is listed in Table I; the agreement of the two calculations is within the expected numerical accuracy. Of course, the agreement of the one-electron band energies with experiment suffers from the well-known problem of local-density theory.[43]

TABLE I. Band characteristics of perfect MgO compared with the calculation of Chang and Cohen (Ref. 39) and with experimental values (Refs. 40 and 41) (units are in eV).

	Band gap	*s-p*-band width	*p*-band width	*s*-band width
Present work	4.36	17.23	4.80	1.83
Chang-Cohen	4.50	17.14	4.80	1.74
Expt.	7.77	20.0	5–6	

The total energy was also calculated according to Eq. (6), and by subtracting the corresponding atomic energies, the cohesive energy of MgO could be determined. In determining the total energy of atomic oxygen, we considered two ways of correcting for the multiplet energy of the oxygen ground state—using the 1.50-eV spin-polarization correction quoted by Chang and Cohen and using a value of 0.94 eV derived from the experimental multiplet splitting.[44] We have also used the 0.144-eV correction for the zero-point vibrational energy of MgO as estimated by Chang and Cohen within the Debye approximation. The agreement between our calculation and that of Chang and Cohen and of the experimental result[42] is within the expected numerical accuracy of our calculations, as shown in Table II. In the same table we also list our results obtained from a completely converged

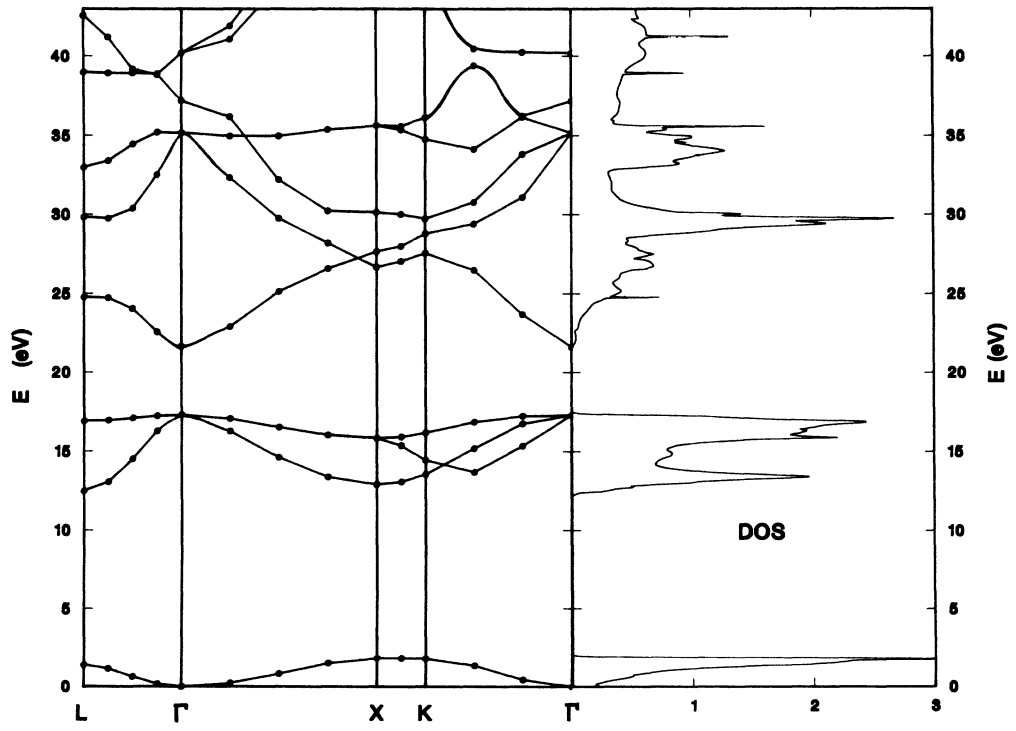

FIG. 2. Band structure and density of states for perfect MgO. The density of states is given in units of states/eV/MgO. The zero of energy is chosen as the minimum level of the oxygen *s* band.

calculation obtained by increasing the cutoff of the reciprocal-lattice vectors sums to $|\mathbf{G}|^2 \leq 256$ bohr^{-2}, and the cutoff energy for the LCAO functions to $|\mathbf{k}+\mathbf{G}|^2 \leq 120$ bohr^{-2}.

The electronic structures of the F centers in MgO crystals were then studied in detail using the techniques discussed above. We present the results for the electronic structure at the relaxed nuclear configuration. In the top panel of Fig. 3 we present the valence-band structure and the related density of states of the neutral F center in MgO using the Mg_8O_7d supercell. As in the calculation for defect-free MgO, the zero of energy in this plot was taken at the bottom of the oxygen s band, which is located at the Γ point. The dotted line in the DOS plot represents the partial density of the F-center impurity states. The PDOS curve indicates that the F-center defect in a MgO crystal introduces impurity states mainly into the MgO band gap as represented by a single band in the band plot.

Due to the finite size of the supercell, the impurity band turns out to be nearly 2 eV wide. In order to approximate the energy E_0 of an isolated impurity, we made the following extrapolation to the results for an infinite supercell. Assuming that the bandwidth can be approximated by interactions between nearest-neighbor vacancy sites, parametrized by the unknown interaction constant E_1, the tight-binding dispersion expression is given by

$$E(\mathbf{k})=E_0+4E_1[\cos(k_x a)\cos(k_y a)+\cos(k_y a)\cos(k_z a)+\cos(k_z a)\cos(k_x a)] , \quad (7)$$

where a is the cubic lattice constant of MgO given in Sec. II A, the eigenvalues at some of the $\mathbf{k}$ points in the supercell Brillouin zone then take the following values:

$$\begin{aligned} E(L)&=E_0 , \\ E(\Gamma)&=E_0+12E_1 , \\ E(X)&=E_0-4E_1 , \\ E(K)&=E_0-3.656\,85E_1 . \end{aligned} \quad (8)$$

Thus, the impurity band is exactly represented by the value E_0 at the L point. The accuracy of Eq. (7), determined by checking the consistency of the relations (8)

TABLE II. Cohesive energy (in eV) of perfect MgO compared with the calculation of Chang and Cohen (Ref. 39) and with experimental value (Ref. 42).

Present work[a]	Present work[b]	Chang-Cohen	Expt.
9.50[c]	10.01[c]	9.96[c]	10.345
10.06[d]	10.56[d]		

[a]Calculated by using the general cutoff of the reciprocal-lattice vectors to be $|\mathbf{G}|^2 \leq 121$ bohr^{-2}, the cutoff energies for the plane-wave basis functions to be $|\mathbf{k}+\mathbf{G}|^2 \leq 8$ bohr^{-2}, and the cutoff energies for the LCAO functions to be $|\mathbf{k}+\mathbf{G}|^2 \leq 100$ bohr^{-2}.

[b]Calculated by using the general cutoff of the reciprocal-lattice vectors to be $|\mathbf{G}|^2 \leq 256$ bohr^{-2}, the cutoff energies for the plane-wave basis functions to be $|\mathbf{k}+\mathbf{G}|^2 \leq 8$ bohr^{-2}, and the cutoff energies for the LCAO functions to be $|\mathbf{k}+\mathbf{G}|^2 \leq 120$ bohr^{-2}.

[c]Calculated using corrections for the zero-point vibrational energy of MgO and the spin-polarization energy of oxygen quoted in Ref. 39.

[d]Calculated using the same correction for zero-point vibrational energy as above, but using the experimental spin-polarization correction for oxygen derived from Ref. 44.

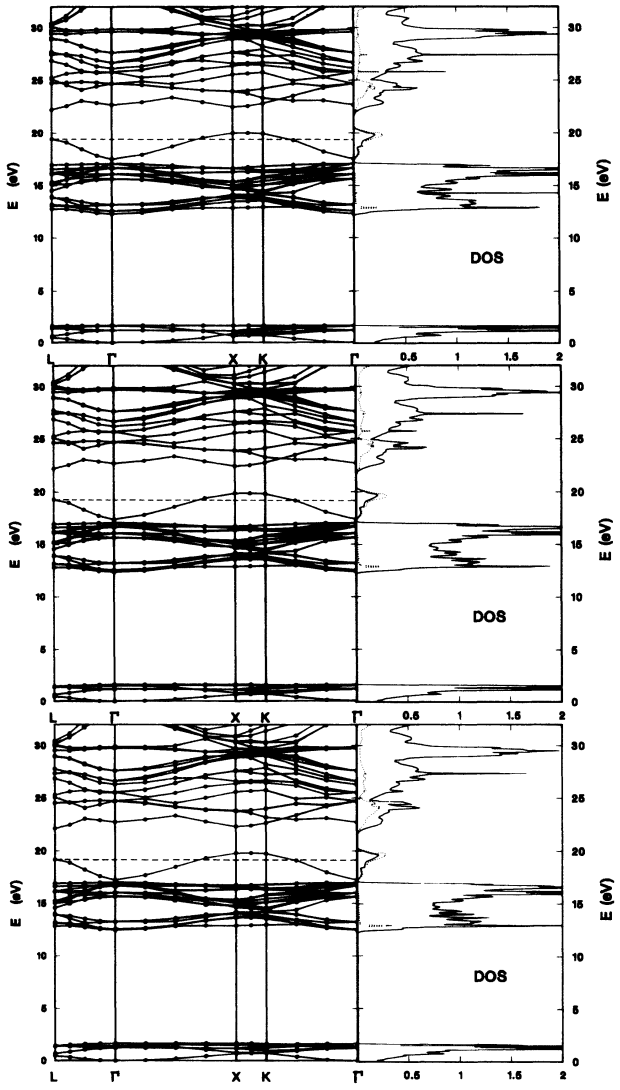

FIG. 3. Band structure and density of states for F, F^+, and F^{2+} centers in MgO crystals as represented by the Mg_8O_7d supercell. The zero of energy is chosen at the bottom of oxygen s band. The impurity level extrapolated to the infinite-supercell value is shown by the dashed lines in the band-structure plots. The density of states (solid lines) is given in units of states/eV/MgO (states/eV/[$(Mg_8O_7d)/8$]). The partial density of states (dotted lines), as defined by Eq. (5), is amplified by a factor of 5. Top panel, neutral F center; middle panel, F^+ center ("excited" treatment); bottom panel, F^{2+} center ("excited" treatment).

with the corresponding band-structure results, was better than 0.1 eV. The extrapolated isolated impurity level of the F center is indicated in Fig. 3 with a dashed straight line in the band plot.

The band calculation for F^+ and F^{2+} centers were also performed, using both the "ionized" and "excited" treatments discussed in Sec. II E, and very similar structures were obtained. The results for the "excited" treatment are presented in Fig. 3, in the middle and bottom panels, respectively, including the extrapolated isolated impurity level and the corresponding density of states. The existence of the impurity band in band gap is apparent for both of these two defects, even in the case of the F^{2+} center, which has no electrons trapped at the oxygen vacancy site. The differences between the electronic structures of the neutral and charged F centers are very slight. There is a small variation in the location of the impurity band within the band gap for the three charge states. The energy difference between the top of the valence band and the extrapolated impurity band is listed in Table III for each of the F-type impurities including the results of both the "ionized" and "excited" treatments for the charged F centers. In the same table, these energies are also compared with the results of the muffin-tin Green's-function calculation obtained by Klein *et al.*[13] The "excited"-treatment results indicate that the impurity band is rigid, varying in energy by less than 0.1 eV. The "ionized"-treatment results indicate that the impurity band shifts closer to the oxygen p valence band with increasing charge. The latter results are similar to those of Klein *et al.*[13]

In addition to the impurity band, the PDOS curves in Fig. 3 indicate that the vacancy site has a small contribution to states near the bottom of the oxygen p band and a larger contribution to states at the bottom of the conduction band. The peak height in the PDOS curve at the bottom of the oxygen p band increases with increasing impurity charge. This increasing hybridization is more pronounced in the "ionized" treatment. The impurity contributions to the bottom of the conduction band are similar in the three charge states. They represent the excited states and *bona fide* resonances of the F centers. Although experimental luminescence results[1–9] as well as the results of several calculations[5,10,13] indicate the presence of discrete excited states for F centers less than 0.1 eV below the conduction-band edge, in our supercell treatment all of these states appear as resonances, hybridized with the conduction band of MgO. Because of the hybridization we are unable to extrapolate the excited impurity bands to the results of an infinite supercell as we did for the ground-state impurity level. However, we expect that the supercell impurity resonances do a reasonable job of representing the average charge distribution of the excited states of the F centers.

TABLE III. Position of F-center impurity band compared with calculation of Klein, Pickett, Boyer, and Zeller (Ref. 13) (energy measured with respect to the top of the valence band of MgO, units are in eV).

	"Excited" scheme	"Ionized" scheme	Klein *et al.*
F center	2.34	2.34	2.10
F^+ center	2.25	1.57	1.22
F^{2+} center	2.19	1.47	

The results of band-structure calculations enable us to study the impurity charge density for each of the defect centers. Contour plots of the occupied impurity states, as represented in the "excited" treatment, is shown in Fig. 4. Figure 4(a) presents the contour plot of the neutral F-center impurity charge density, showing the behavior of the two trapped electrons in the impurity band within the band gap. Figures 4(b) and 4(c) show impurity charge-density contours for the F^+ center, the former showing the contribution of the single trapped electron in the impurity band within the band gap and the latter showing the contribution of the electron excited to the conduction-band resonance. Figure 4(d) shows the contour plot for the F^{2+} center, corresponding to the charge density of the two electrons excited to the conduction-band resonance. These contours were all plotted in the (100) plane of the supercell, passing through the vacancy site located at the center. The same contour levels were used in the four plots. Four nearest-neighbor Mg atoms at their relaxed positions, as well as four nearest-neighbor and four next-nearest-neighbor oxygen atoms, are also shown in this plot. These results indicate that the charge of impurity centers is not only distributed at the vacancy sites (the center and the four corners in each plot), but also has contributions at the oxygen sites. The lowest impurity state [Figs. 4(a) and 4(b)] has a local maximum at the impurity site and is highly concentrated on the nearest O neighbors. The excited impurity state [Figs. 4(c) and 4(d)] has a local minimum at the impurity site, and is more uniformly spread throughout the unit cell. In general, we find the shapes of the contours of a given one-electron state to be very similar for the F, F^+, and F^{2+} centers.

Contours plots of the total valence charge density $\rho(\mathbf{r})$ for the three types of F centers were also plotted in the same plane as above and are shown in Fig. 5. The contour levels were chosen in order to see the charge distribution near the impurity site; the peak densities at the oxygen sites were too large to be seen on this scale and were omitted from the plot. These peak densities were 7.03, 7.05, and 7.08 electrons/Å^3 for the F, F^+ and F^{2+} centers, respectively. The 0.1 electron/Å^3 contour level distinguishes the three cases, although unfortunately it is subject to noise in the total-density calculation. Looking at Figs. 5(a) and 5(b), the singly charged F^+ center shows more charge concentration at the vacancy site. This can be seen from the presence of the 0.1 electron/Å^3 contour close to the impurity site in Fig. 5(b) (modulated by the noise of the calculation), while that contour is further from the impurity site in Fig. 5(a). Physically, this can be explained by the attractive Coulomb potential at the impurity site caused by the surrounding Mg^{2+} ions. For the neutral F center, the two trapped electrons screen the attractive potential from each other. For the F^+ center, only a single electron is present to respond to the attrac-

TABLE IV. Relaxation distance and corresponding relaxation energy for each type of impurity in MgO.

	"Excited" scheme			"Ionized" scheme			
	F	F^+	F^{2+}	F^+	F^{2+}	H^{2-}	H^-
Relaxation distance (%)	−0.9	0.25	1.9	0.06	2.06	0.3	0.13
Relaxation energy (eV)	0.03	0.006	0.11	0.0001	0.13	0.04	0.0005

tive potential at the vacancy sites. For the F^{2+} center [Fig. 5(c)] both electrons have been excited to extended states.

The total energies of the F centers were calculated as described in Sec. II D. For the neutral F center, our calculations could be compared with the experimentally determined formation energy of the defect. By subtracting the total energy of a pure MgO crystal plus that of an excess Mg atom from the total energy of the relaxed Mg_8O_7d supercell, the formation energy could be estimated according to the equation

$$E_{\text{formation}} = E_{\text{tot}}(Mg_8O_7d) - [7E_{\text{tot}}(MgO) + E_{\text{tot}}(Mg)] . \quad (9)$$

The resulting formation energy of the F center was deter-

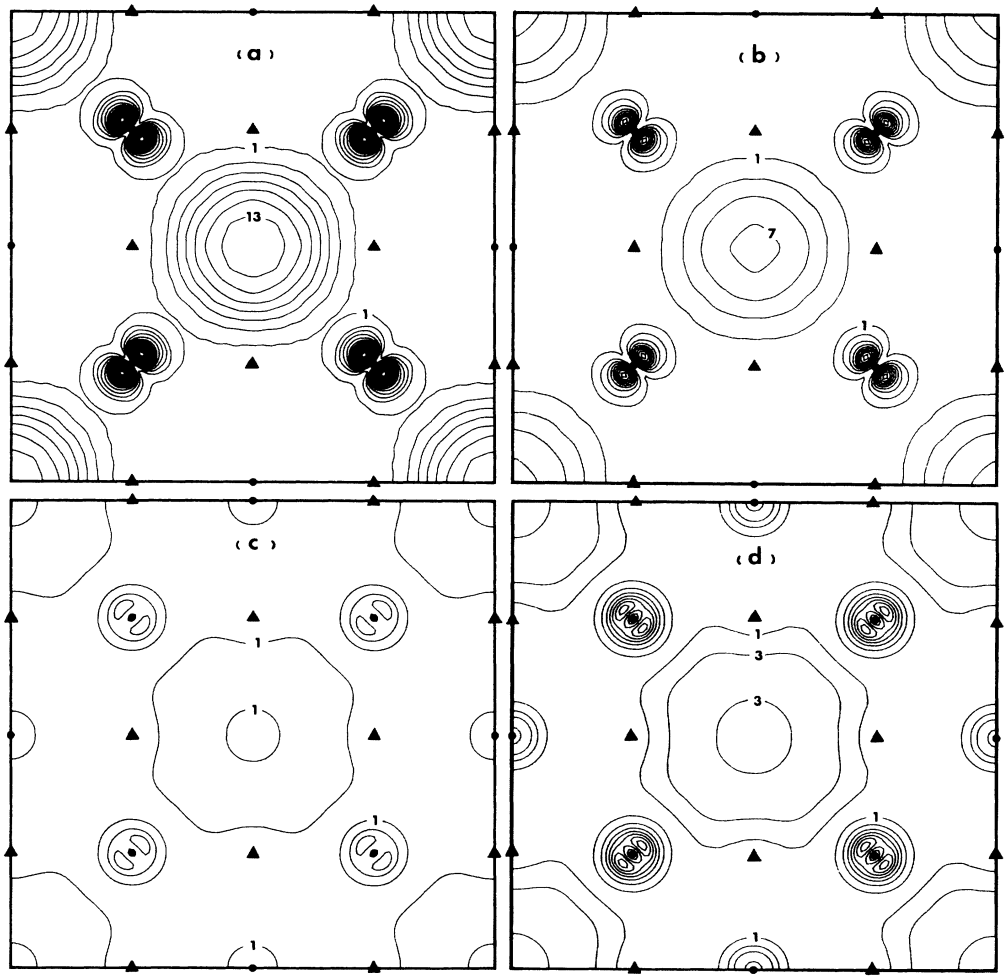

FIG. 4. Impurity charge-density contours for F, F^+, and F^{2+} centers in MgO. The magnesium sites are represented by triangles; the oxygen sites are represented by dots. The contour values in each panel are in units of 0.01 electron/Å^3, and contour levels are equally spaced in intervals of 0.02 electron/Å^3. (a) Charge density of two electrons within the impurity band of the F center. (b) Charge density of a single electron within the impurity band of the F^+ center ("excited" treatment). (c) Charge density of a single electron within the conduction band of the F^+ center ("excited" treatment). (d) Charge density of two electrons within the conduction band of the F^{2+} center ("excited" treatment).

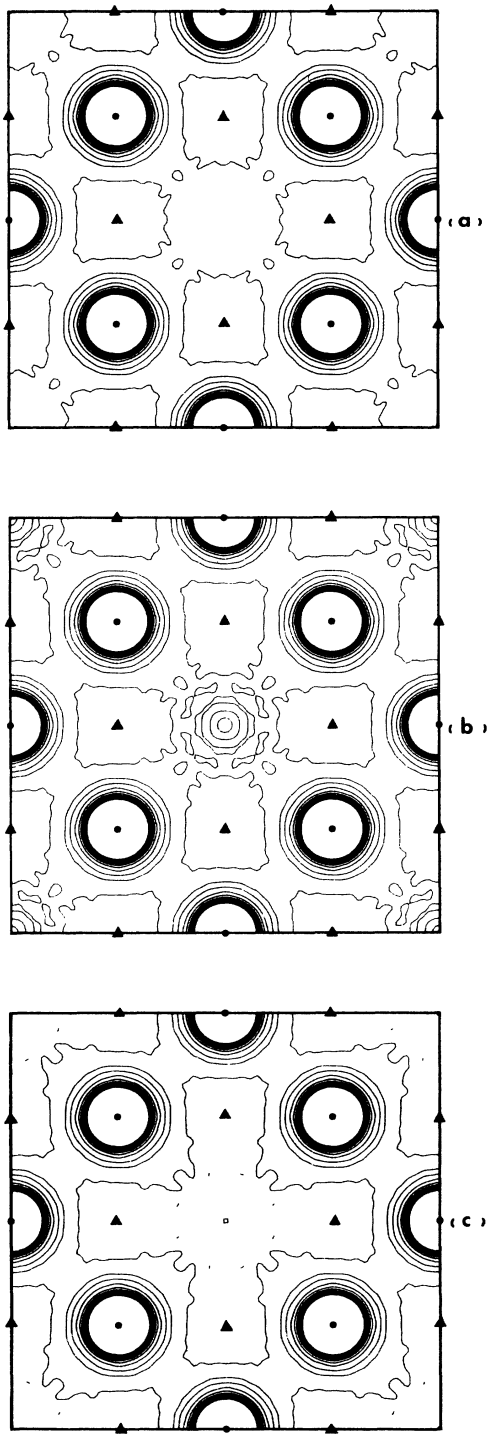

FIG. 5. Total valence charge density for F, F^+, and F^{2+} center in MgO. The magnesium sites are represented by triangles; the oxygen sites are represented by dots. The contour values in every panel are in units of 0.1 electron/Å^3, contour levels are equally spaced in intervals of 0.2 electron/Å^3, and the density peaks in each plot were cut off in the high-density regions near the oxygen sites. (a) Total valence charge-density distribution of the F center in MgO. (b) Total valence charge-density distribution of the F^+ center ("excited" treatment) in MgO. (c) Total valence charge-density distribution of the F^{2+} center ("excited" treatment) in MgO.

mined to be -0.4 eV. This quantity was reported in early experimental work by Kappers, Kroes, and Hensley.[45] They colored the MgO crystals by heating them in Mg vapor. Determining the density of F centers at fixed temperature as a function of Mg vapor density, they estimated the F-center–formation energy in MgO to be -1.53 eV. Our calculated formation energy is more than 1 eV smaller than the experimental result. However, this calculation is close to the limit of our accuracy. From the results of the cohesive energy of MgO, we have found that our absolute convergence error is 0.5 eV. The relative error is less than that; estimating the relative error of each calculated term in Eq. (9) to be 0.1 eV, we can account for most of the discrepancy. In addition, as discussed below, the constraints of our supercell have caused us to underestimate the relaxation energy of the defect and hence to underestimate the formation energy (9).

For each type of impurity, the total-energy calculation was carried out at several small relaxations of the nearest Mg^{2+} neighbors around the vacancy site while maintaining the O_h point-group symmetry. The total energy could then be interpolated as a polynomial function of the fractional relaxation of these Mg^{2+} ions. The total-energy configuration-coordinate diagrams for the F, F^+, and F^{2+} centers are presented in Fig. 6, where the ionized impurities were evaluated in the "excited" scheme. After minimizing each of the total-energy polynomials, the relaxation distance of the nearest shell of Mg^{2+} ions

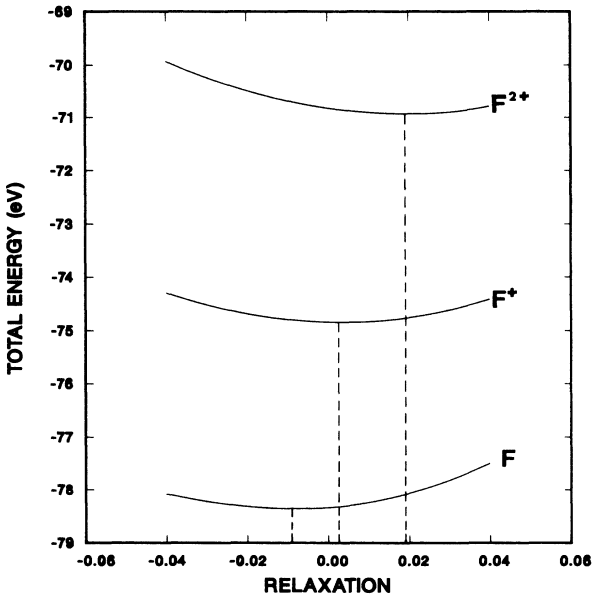

FIG. 6. Total-energy configuration-coordinate diagram for F, F^+, and F^{2+} centers ("excited" treatment) in MgO. The total energy for each defect is presented as a function of fractional relaxation of the nearest Mg^{2+} neighbors around the oxygen vacancy site. The lowest total energy corresponds to -0.9%, 0.25%, and 1.9% relaxation of the nearest Mg^{2+} neighbors for the F, F^+, and F^{2+} centers, respectively.

and the corresponding relaxation energies were obtained and listed in Table IV. The fractional relaxation distances are also indicated in Fig. 6. These results indicate that for the F center the lowest total energy corresponds to a small amount ($\sim 0.9\%$) of inward relaxation of the nearest Mg^{2+} neighbors toward the vacancy site; for the F^+ center, the equilibrium position of the nearest Mg^{2+} shell is very close to the original configuration with just a slight expansion ($\sim 0.25\%$); for the F^{2+} center, the total energy minimized at about 1.9% outward relaxation of the nearest Mg^{2+} ions away from the vacancy site. The results obtained in the "ionized" scheme differ slightly, as indicated in Table IV. Since the relaxation energies summarized in Table IV are so very small, they are close to the limits of accuracy for the calculations and therefore should be considered only qualitatively. The configuration-coordinate results agree qualitatively, but not quantitatively, with the schematic curves shown in Fig. 1 and the calculated results of previous workers. The Franck-Condon transitions corresponding to the results of Fig. 6 are all approximately 4 eV for all absorption and emission processes. This is a relatively small difference from the experimentally observed value of 5 eV for both the $F \rightarrow F^+$ and $F \rightarrow F^{2+}$ absorption processes, but a somewhat larger difference from the observed values of 3 and 2 eV for the $F^{2+} \rightarrow F^+$ and $F^+ \rightarrow F$ emission processes, respectively. The reasons for this discrepancy are discussed in Sec. V.

IV. ELECTRONIC STRUCTURE OF HYDROGEN IMPURITIES IN MgO

In order to complete the study of vacancy defects in MgO, we studied the electronic structure of the electron-trap sites—singly charged H^- and neutral H^{2-}—using the same calculational techniques as described in Sec. II. In this case the supercell stoichiometry was Mg_8O_7H.

The band structure of the neutral H^{2-} defect in the supercell Brillouin zone is shown in the top panel of Fig. 7, along with the corresponding density of states. Again, the dotted line gives the partial density of the impurity states. This partial density curve tells us clearly that the neutral H^{2-} defect (a H^+ ion with three trapped electrons) removes the vacancy ground state from the band gap down to below and within the oxygen p band of MgO. The peak in the DOS just below the oxygen p band can be denoted to be the lowest hydrogen impurity band corresponding to the filled H $1s$ states. In addition to these contributions, the PDOS curve shows significant contributions near the bottom of the conduction band. Although the experimental evidence[5] suggests the existence of a bound state 0.56 eV below the bottom of the conduction band, this state appears as a resonance in the supercell treatment, similar to the F-center resonance discussed above. For H^{2-}, this resonance state is occupied by one electron.

In order to study the hydrogen impurity states in more detail, we have constructed contour plots corresponding to the hydrogen bands. In Figs. 8(a) and 8(b) we show the density contours, plotted in the same plane as in Figs. 4 and 5, for the low-lying H $1s$ band and for the H resonance in the conduction band, respectively. As shown in Fig. 8(a), the hydrogen $1s$ band is hybridized with oxygen p states on the nearest oxygen sites. As shown in Fig. 8(b), the H resonance state has a charge density that is similar to that of vacancy resonance state shown in Fig. 4(c).

The bands and the density of states of the singly charged H^- defect in MgO have been calculated using both the "excited" and "ionized" schemes as described in Sec. II E. Both results are very close to those for the neutral H^{2-} defect. The results for the "excited" treatment of H^- are almost indistinguishable from the ground-state results of neutral H^{2-}. This is not surprising since the "excited" electron is taken from the bottom conduction band and placed in the next-available conduction-band state which has a very similar distribution. For H^-, the "ionized" treatment is better defined, requiring no occupancy of conduction-band states. These results are presented in the lower panel of Fig. 7. Small energy

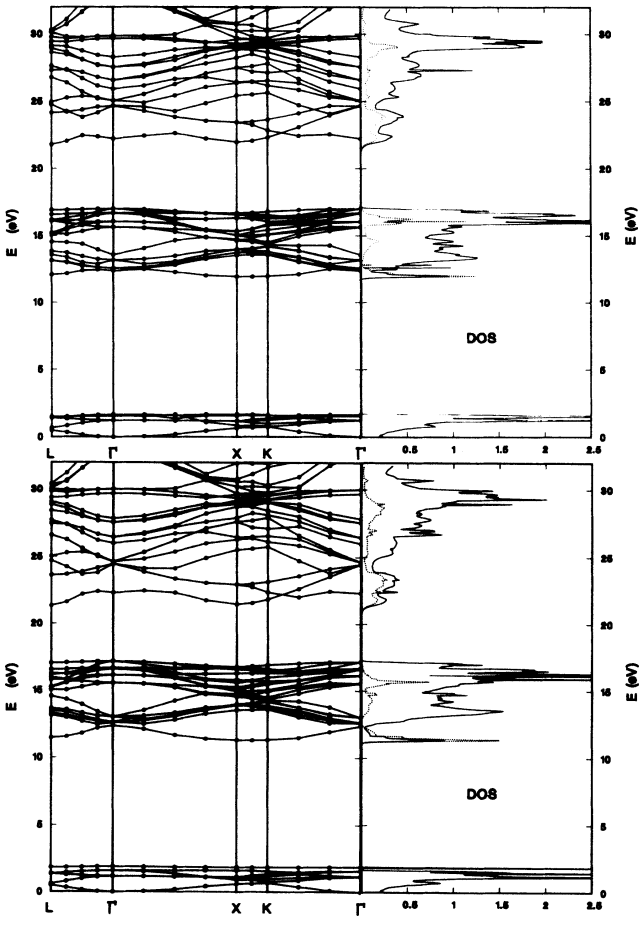

FIG. 7. Band structure and density of states for H^{2-} and H^- defects in MgO. The zero of energy is chosen at the bottom of the oxygen s band. The density of states (solid line) is given in units of states/eV/MgO (states/eV/[$(Mg_8O_7H)/8$]). The partial density of hydrogen impurity states (dotted line), as defined by Eq. (5), is amplified by a factor of 5. Top panel, neutral H^{2-} defect; bottom panel, H^- ("ionized" treatment).

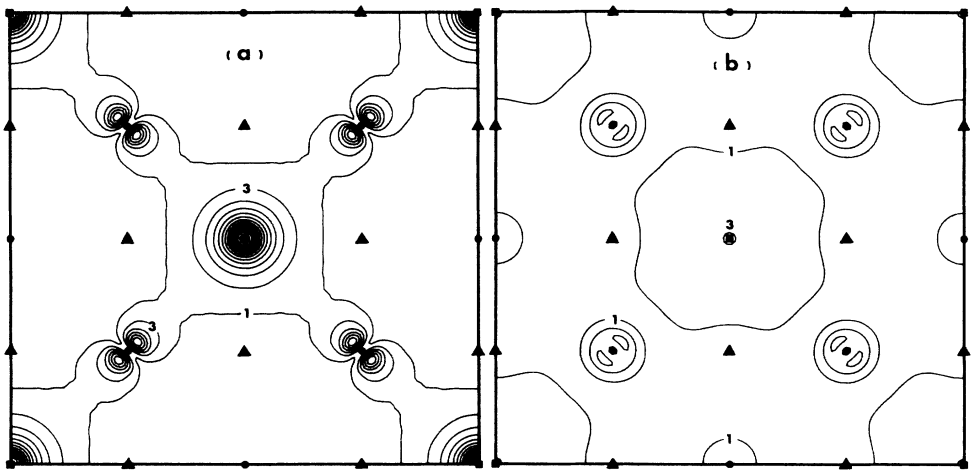

FIG. 8. Impurity charge-density contours for the H^{2-} defect in MgO. The triangles indicate magnesium sites, the dots indicate oxygen sites, and the squares indicate hydrogen sites. The contour values in each panel are in units of 0.01 electron/Å^3, and contour levels are equally spaced in intervals of 0.02 electron/Å^3. (a) Hydrogen impurity charge density of the H^{2-} defect contributed by the one-electron state below the oxygen p band. (b) Hydrogen impurity charge density of the H^{2-} defect contributed by first-excited one-electron state within the conduction band.

shifts can be seen in the comparison of the H^- results with those of neutral H^{2-}. In general, the H-like states move to slightly lower energy, including both the hydrogen 1s state at the bottom of the oxygen p band and the resonance impurity band at the bottom of the conduction band. This is probably the result of electrostatic screening effects.

The total valence charge-density contours for H^{2-} and ionized H^- defects in Fig. 9 were plotted in the same plane, with the same contour levels as for the F-center results in Fig. 5. The peak densities near the oxygen sites have been omitted from the plot, they are both a little higher than that of the F center at 7.04 electrons/Å^3 for H^{2-} and 7.07 electrons/Å^3 for H^-. The plot demonstrates the existence of the hydrogen impurities at the oxygen vacancy sites and, moreover, shows that, for the charged H^- defect the valence charge is more contracted toward the impurity sites than for the neutral H^{2-} defect.

The configuration-coordinate diagram for H^- (ionized) and H^{2-} defects in MgO were studied using the same approach as for the F centers. Generally, the total energy at each relaxation position is a few electron-volts lower than for the F center, which confirms the stability of the hydrogen binding to the oxygen vacancy sites in MgO. One can see from Fig. 10 that for both charge states the lowest level of total energy corresponds to different small amounts of expansion of the nearest Mg^{2+}-ion neighbors. The relaxation distances and relaxation energies are given in Table IV. The distance between the two total-energy configuration curves for H^{2-} and H^- defects is small, which is consistent with the experimental notion[5] that the H^- defect is a shallow trapping site and the H^{2-} defect provides a reservoir of electrons released with thermal energy according to the process $H^- + e^- \leftrightarrow H^{2-}$.

V. DISCUSSION AND CONCLUSIONS

In this work we set out to examine the model illustrated in Fig. 1, describing the relationships between different charge states of F centers in MgO crystals, and also to examine the substitutional hydrogen defects within the same framework. Density-functional theory has enabled us to examine both the one-electron spectrum and the total energy of the system at the same time. In general, our results are in qualitative agreement with existing experimental evidence and in qualitative agreement with recent theoretical calculations. As discussed below, the lack of quantitative agreement is mainly due to the use of a small supercell. The advantage of the supercell treatment is that it enables one to use well-developed computational techniques to study nonperiodic systems. The price one pays for this convenience is that in order to obtain physically meaningful results, one must extrapolate the small-supercell results to that of an infinite supercell. This we were able to to do for the one-electron energy of the ground-state impurity band. It is unfortunately not possible to simply carry out such an extrapolation for the excited one-electron states of the impurities, nor for the total energies of the systems.

Despite the lack of quantitative agreement, we have learned quite a lot about the defect states. Figure 11 summarizes the main results from the one-electron spectrum of the neutral defects. In this figure the DOS for pure MgO is given in the top plots, below which are shown the DOS and PDOS for the neutral F (top panel) and for the neutral H^{2-} defect (bottom panel). Both impurities introduce resonances at the bottom of the conduction band. The F center introduces an impurity band into the band gap, while the hydrogen center contributes

its states within the oxygen p bands, including a H $1s$ band just below the oxygen p bands. The charge-density contour plots of Figs. 4 and 8 enabled us to examine the nature of these states in detail for the neutral defects as well as for their charged counterparts.

We have examined two different schemes for treating charged impurities, which we have called the "ionized" and "excited" treatments. In the former treatment, the ground state of the charged system is determined self-consistently with divergences in the Coulomb interaction removed and approximate energy shifts applied. In the latter treatment, an excited state of the neutral system is calculated self-consistently by applying constraints to the occupation numbers of the one-electron states. For calculating the total energy of the charged F centers F^+ and F^{2+}, the "excited" treatment, which is similar to the ΔSCF approach, is much better defined. It, in principle, contains many of the effects needed for a full many-body treatment of the excitation process.[43] For calculating the one-electron spectrum, the two approaches bracket the screening effects expected for the charged F centers F^+ and F^{2+}: the "ionized" treatment representing the absence of screening by the conduction electron and the "excited" treatment representing full screening by the conduction electron. Since the "conduction electron" has an admixture of the resonance states of the impurity, the screening of the "excited" treatment is perhaps slightly overestimated relative to the screening by a *bona fide* conduction electron. The results for the "excited" treatment of the charged F centers, presented in Sec. III, show that the one-electron states are quite rigid with respect to their charge state. The results of the "ionized" treatment of the charged F centers F^+ and F^{2+}, mentioned in Tables III and IV, show small energy shifts. For the hydrogenated vacancy, the situation is complicated by the absence of a well-defined impurity level in the excited state. In this case the "excited" treatment involves removing an electron from the conduction-band resonance and placing it in a higher conduction-band state. The procedure is not very well defined, and leads to results that are nearly indistinguishable from those of

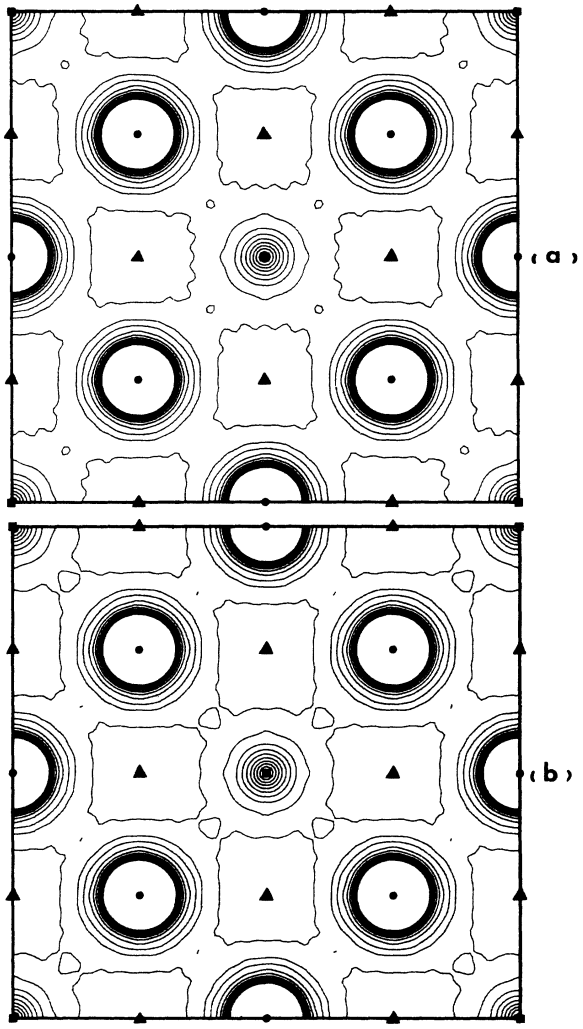

FIG. 9. Total valence charge density for H^{2-} and H^- defects in MgO. The magnesium sites are represented by triangles, the oxygen sites are represented by dots, and the hydrogen sites are represented by squares. The contour values are all in units of 0.1 electron/Å^3, and contour levels are equally spaced in intervals of 0.2 electron/Å^3. The density peaks in each plot were cut off in the high-density regions near the oxygen sites. (a) Total valence charge-density distribution for the H^{2-} defect in MgO. (b) Total valence charge-density distribution for the H^- defect ("ionized" treatment) in MgO.

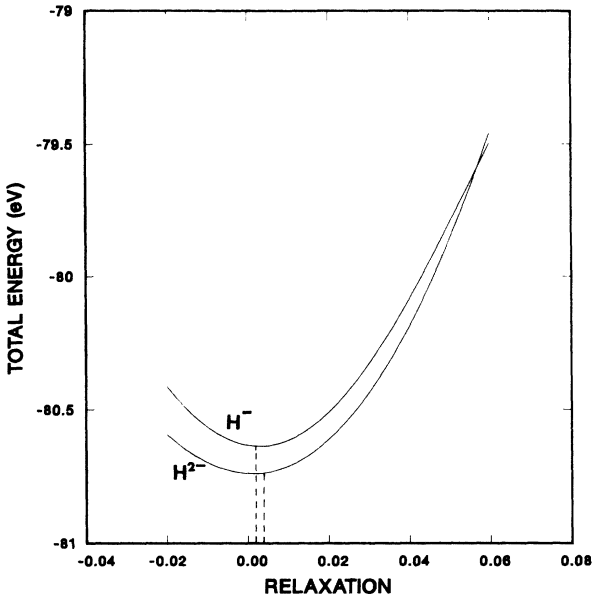

FIG. 10. Total-energy configuration-coordinate diagram for H^{2-} and H^- defects ("ionized" treatment) in MgO. The total energy for each defect is presented as a function of the fractional relaxation of the nearest Mg^{2+} neighbors around the hydrogen impurity site. The lowest total energy corresponds to a small amount (0.28% for H^{2-}, 0.13% for ionized H^-) of expansion of the nearest Mg^{2+}-ion shell away from the impurity site.

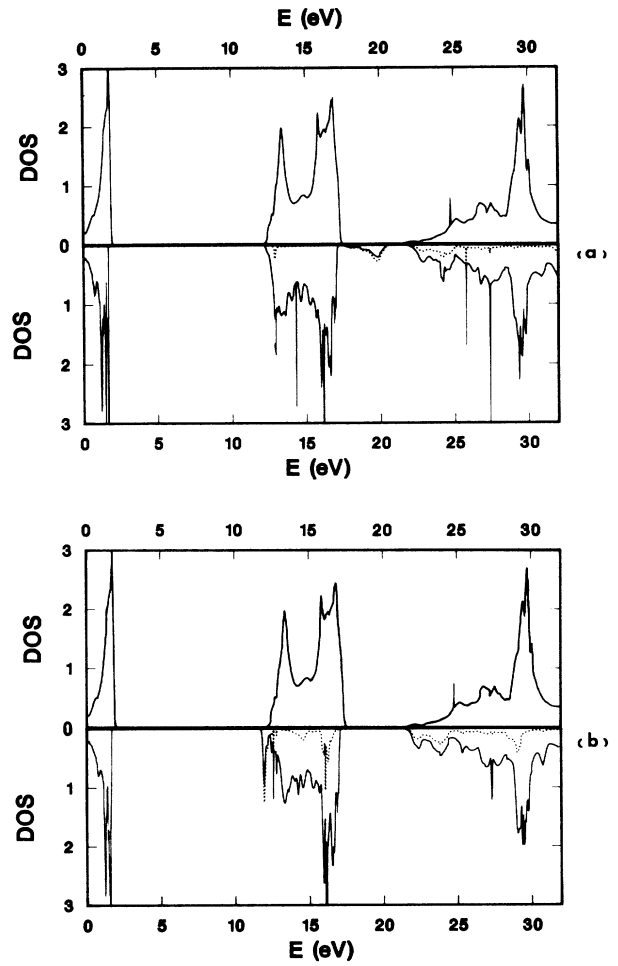

FIG. 11. (a) Comparison of the density of states of the F center in MgO (lower plot) with that of perfect MgO (upper plot). (b) Comparison of the density of states of the H^{2-} defect in MgO (lower plot) with that of perfect MgO (upper plot). The PDOS for the impurity sites, amplified by a factor of 5, is indicated in both lower plots with a dotted line. DOS are given in units of states/eV/MgO.

the neutral H^{2-} defect. Therefore, only the results for the "ionized" treatment are presented in Sec. IV.

Although the F and F^+ centers have been discussed in the theoretical literature,[10,13–15] to our knowledge the existence of the doubly charged F^{2+} centers has not been verified.[11,12] The band-structure and DOS diagrams in the bottom panel of Fig. 3 clearly show that the F^{2+} defect has well-defined (although unoccupied) one-electron impurity band within the band gap. This one-electron impurity band is, in fact, very similar for the three charge states F, F^+, and F^{2+}.

In our study of the lattice relaxation about the defect site, our results have qualitative similarities to those of Pandey and Vail,[15] although there are large quantitative differences. In general, our calculated relaxation energies and distances have the same sign, but are considerably smaller than those of Pandey and Vail.[15] In addition to the discrepancy with other theoretical work, our relaxation results disagree in some respects with the experimental evidence shown schematically in Fig. 1. The results of the configuration-coordinate diagram shown in Fig. 6 generally show that the variation of the total energy with lattice relaxation is too small to be consistent with the photon absorption and emission energies.[5] We believe that the largest source of this discrepancy is the geometrical constraint placed on the system by the small supercell. Pandey and Vail[15] found that a significant amount of the relaxation energy is contributed by the nearest-neighbor O^{2-} ions in addition to the nearest-neighbor Mg^{2+} ions. In our supercell treatment, only the nearest-neighbor Mg^{2+} ions can relax; the nearest-neighbor O^{2-} ions are equidistant from two defect sites and therefore cannot relax. In the present formalism, one could model some of the effects of the O^{2-} relaxation by allowing the supercell dimensions to be a relaxation variable. We have not investigated this possibility.

The fact that the configuration-coordinate diagram of Fig. 6 is qualitatively similar to the model discussed by Rosenblatt *et al.*[9] helps establish its plausibility. Briefly, Rosenblatt *et al.*[9] illuminated MgO crystals containing F and F^+ centers with a pulse of 5-eV radiation and detected the luminescence at a series of delay times. For the crystal sample ("MgO I") of Ref. 9 containing the highest concentration of hydrogen as well as a large concentration of oxygen vacancies, they first detected predominantly 3-eV luminescence, and then at longer times, extending to several millisecond, detected predominantly 2-eV luminescence. In addition, for the same sample, they studied the luminescence spectrum as a function for the power density in the 5-eV excitation pulse. In this case, both 3- and 2-eV luminescence were observed at high power densities, while mainly 2-eV luminescence was observed at the lowest power density. The 3-eV radiation comes from the $F^{2+} \rightarrow F^{+*} \rightarrow F^+$ transition (sometimes referred to as F^+ luminescence). The 2-eV radiation comes from the $F^+ \rightarrow F^* \rightarrow F$ transition (sometimes referred to as F luminescence). These results point to the notion that the $F^{+*} \leftrightarrow F^{2+}$ state is the highest-energy state of the F-center system. Under intense 5-eV illumination, the majority of the oxygen vacancies can be excited to this top state. These states then luminesce with 3-eV radiation to increase the population of $F^+ \leftrightarrow F^*$ states. These states then luminesce with 2-eV radiation back down to the ground state. Under less intense 5-eV illumination, mainly the $F^+ \leftrightarrow F^*$ state is excited and only 2-eV luminescence is observed. Hydrogen trap sites play an important role in this simple picture by effectively increasing the time that the defect can remain in the F^+ state, facilitating the excitation to the $F^{+*} \leftrightarrow F^{2+}$ state in a two-step procedure which would otherwise require a two-photon process. The hydrogen trap sites also effectively increase the lifetime of the $F^{+*} \leftrightarrow F^{2+}$ state, which has been observed to persist for seconds after illumination. Since hydrogen trap sites can simultaneously provide a reservoir of electrons for both

the F^{2+} and F^{+} centers, the observed similarity between the time dependences of the 3- and 2-eV luminescences is consistent with this model.[9] Samples having lower concentrations of hydrogen trap sites exhibit a more complicated behavior, suggesting the presence of several defect environments. In these crystals, one can observe the sequence of deexcitation from initially 3-eV luminescence to later 2-eV luminescence occurring within much shorter time scales, ranging from nanoseconds or microseconds, depending on the sample. Superimposed on the rapid decay sequences, one also observes the slower decay sequence similar to that seen in the hydrogen-regulated processes of the "MgO I" crystal of Ref. 9. It might be possible to quantify these ideas by developing kinetic equations based on this model.

In summary, we have demonstrated that self-consistent density-functional theory is capable of describing both the one-electron spectrum and the total energy of F, F^{+}, F^{2+}, H^{2-}, and H^{-} defects in MgO crystals. In the one-electron results, we demonstrated that in all three charge states of the oxygen vacancy in MgO there is well-defined impurity level within the band gap. For the hydrogenated oxygen vacancy the gap state is removed and hydrogen resonances are found within the valence and conduction bands of MgO. In the total-energy results, we constructed a configuration-coordinate diagram for each of the defects. The diagram for the F, F^{+}, and F^{2+} defects is qualitatively similar to the model proposed in Fig. 1. The diagram for the H^{2-} and H^{-} impurities is consistent with the notion that the process $H^{2-} \leftrightarrow H^{-} + e^{-}$ provides an electron-trap site and electron reservoir for electrons released into the conduction band. In order to make these results more quantitative, it will be necessary to go beyond the small-supercell approximation.

ACKNOWLEDGMENTS

We would like to acknowledge helpful conversations with R. T. Williams, G. P. Williams, Jr., Y. Chen, Y. Bar-Yam, R. Pandey, J. M. Vail, and T. M. Wilson. This work was partially supported by U.S. National Science Foundation (NSF) under Grant No. DMR-85-01022, and by the William C. Archie Fund from Wake Forest University.

*Present address: Department of Physics, North Carolina State University, Raleigh, NC 27695-8202.

[1]W. Hayes and A. M. Stoneham, *Defects and Defect Processes in Nonmetallic Solids* (Wiley, New York, 1985).
[2]B. Henderson, CRC Crit. Rev. Solid-State Mater. Sci. **9**, 1 (1980).
[3]B. T. Jeffries, R. Gonzalez, Y. Chen, and G. P. Summers, Phys. Rev. B **25**, 2077 (1982).
[4]Y. Chen, R. Gonzalez, O. E. Schow, and G. P. Summers, Phys. Rev. B **27**, 1276 (1982).
[5]G. P. Summers, T. M. Wilson, B. T. Jeffries, H. T. Tohver, Y. Chen, and M. M. Abraham, Phys. Rev. B **27**, 1283 (1983).
[6]J. Tombrello, H. T. Tohver, Y. Chen, and T. M. Wilson, Phys. Rev. B **30**, 7374 (1984).
[7]K. Chakrabarti and G. P. Summers, Phys. Lett. A **120**, 466 (1987).
[8]V. M. Orera and Y. Chen, Phys. Rev. B **36**, 5576 (1987); **36**, 6120 (1987).
[9]G. H. Rosenblatt, M. W. Rowe, G. P. Williams, Jr., R. T. Williams, and Y. Chen, Phys. Rev. B **39**, 10 309 (1989).
[10]T. M. Wilson and R. F. Wood, J. Phys. (Paris) Colloq. **37**, C7-190 (1976).
[11]S. Choi and T. Takeuchi, Phys. Rev. Lett. **50**, 1474 (1983).
[12]J. C. Kemp and V. I. Neeley, Phys. Rev. **132**, 215 (1963); T. M. Wilson (private communication).
[13]B. M. Klein, W. E. Pickett, L. L. Boyer, and R. Zeller, Phys. Rev. B **35**, 5802 (1987).
[14]J. M. Vail, A. H. Harker, J. H. Harding, and P. Saul, J. Phys. C **17**, 3401 (1984).
[15]R. Pandey and J. M. Vail, J. Phys. Condens. Matter **1**, 2801 (1989).
[16]R. F. Wood and T. M. Wilson, Phys. Rev. B **15**, 3700 (1977).
[17]R. F. Wood and H. W. Joy, Phys. Rev. **136**, A451 (1964).
[18]R. F. Wood and U. Opik, Phys. Rev. **179**, 783 (1969).
[19]U. Opik and R. F. Wood, Phys. Rev. **179**, 772 (1969).
[20]P. Hohenberg and W. Kohn, Phys. Rev. **136**, B864 (1964); W. Kohn and L. J. Sham, *ibid.* **140**, A1133 (1965).
[21]Q. S. Wang, M. Sc. thesis, Wake Forest University, 1989.
[22]S. G. Louie, K. M. Ho, and M. L. Cohen, Phys. Rev. B **19**, 1774 (1979).
[23]*Crystal Data Determinate Tables,* edited by J. D. H. Donnay and H. M. Ondik (U.S. Department of Commerce, Washington, D.C., 1973), Vol. 2, p. C-57.
[24]L. Hedin and B. I. Lundqvist, J. Phys. C **4**, 2064 (1971).
[25]S. G. Louie, S. Froyen, and M. L. Cohen, Phys. Rev. B **26**, 1738 (1982).
[26]D. R. Hamann, M. Schlüter, and C. Chiang, Phys. Rev. Lett. **43**, 1494 (1979).
[27]G. P. Kerker, J. Phys. C **13**, L189 (1980).
[28]L. Kleinman, Phys. Rev. B **21**, 2630 (1980).
[29]G. B. Bachelet and M. Schlüter, Phys. Rev. B **25**, 2103 (1982).
[30]G. Gilat and L. J. Raubenheimer, Phys. Rev. **144**, 390 (1966).
[31]G. Gilat and Z. Kam, Phys. Rev. Lett. **14**, 715 (1969).
[32]N. A. W. Holzwarth, Q. S. Wang, and S. D. Had, Phys. Rev. B **38**, 3722 (1988).
[33]H. Hellmann, *Einführung in die Quantenchemie* (Deuticke, Leipzig, 1937), p. 285; R. P. Feynman, Phys. Rev. **56**, 340 (1939).
[34]J. Ihm, Rep. Prog. Phys. **51**, 105 (1988).
[35]P. P. Ewald, Ann. Phys. (Leipzig) [Folge 4] **64**, 253 (1921).
[36]Y. Bar-Yam, and J. D. Joannopoulos, Phys. Rev. Lett. **52**, 1129 (1984).
[37]Y. Bar-Sham, and J. D. Joannopoulos, Phys. Rev. B **30**, 1844 (1984); **30**, 2216 (1984).
[38]A. R. Williams and U. von Barth, in *Theory of the Inhomogeneous Electron Gas,* edited by S. Lundqvist and N. H. March (Plenum, New York, 1983), p. 189.
[39]K. J. Chang and M. L. Cohen, Phys. Rev. B **30**, 4774 (1984).
[40]D. M. Roessler and W. C. Walker, Phys. Rev. **159**, 733 (1967).
[41]L. Fiermans, R. Hoogewijs, G. de Mayer, and J. Vennik, Phys.

Status Solidi A **59**, 569 (1980).

[42]*CRC Handbook of Chemistry and Physics,* 60th ed., edited by R. C. Weast and M. J. Astle (Chemical Rubber Co., Boca Raton, FL, 1980), p. D-72.

[43]M. S. Hybertsen and S. G. Louie, Comment. Condens. Matter Phys. **13**, 223 (1987).

[44]C. E. Moore, *Atomic Energy Levels,* Nat. Bur. Stand. (U.S.) Ref. Data Ser. No. 35 (U.S. GPO, Washington, D.C., 1971), Vol. I, p. 45.

[45]L. A. Kappers, R. L. Kroes, and E. B. Hensley, Phys. Rev. B **1**, 4151 (1970).